substance: Dy_2S_3
property: crystal structure, physical properties

α-Dy_2S_3

crystal structure	orthorhombic (D_{2h}^{16} – Pnma)		
lattice parameters			
a	7.279(2) Å		68S
b	15.136(2) Å		
c	3.878(2) Å		

δ-Dy_2S_3

crystal structure	monoclinic (C_{2h}^{2} – $P2_1/m$)		
lattice parameters			
a	17.496(4) Å	color: green	68S
b	4.022(2) Å		
c	10.183(3) Å		
β	98.67°		
melting point			
T_m	1470°C		60P
electrical conductivity			
σ	500 Ω^{-1} cm^{-1}		68S
activation energy for conductivity			
E_A	0.34 eV		68S
Seebeck coefficient			
S	4000 μV K^{-1}	(referred to lead)	68S

γ-Dy_2S_3

crystal structure	cubic (Th_3P_4-defect structure, T_d^6 – $I\bar{4}3d$)		
lattice parameters			
a	8.292 Å		85Z
	8.292 Å		60P
	8.285 Å		81K
melting point			
T_m	1490°C		60P
	1780°C		81K

energy gap and other energy parameters

E_g	3 eV		optical absorption edge	70H
	> 3.8 eV		optical determination	82B
	2.5 ± 0.1 eV		optical gap	85Z
	0.5 eV		X-ray spectra	83S
dE_g/dT	$4.8 \cdot 10^{-4}$ eV/K	T = 250 K...350 K		79Z
E_b	5.8 eV	S 3p-level	MgKα XPS, Fig. 10 (E_b rel. to E_F)	91K
	10 eV	Dy 4f-level	MgKα XPS, Fig. 10	
	14.5 eV	S 3s-level	MgKα XPS, Fig. 10	
	24.5 eV	Dy $5p_{3/2}$-level	MgKα XPS, Fig. 10	
	29.9 eV	Dy $5p_{1/2}$-level	MgKα XPS, Fig. 10	
	43 eV	Dy 5s-level	MgKα XPS, Fig. 10	
	153 eV	Dy $4d_{5/2}$-level	MgKα XPS, Fig. 11	
	158 eV	Dy $4d_{3/2}$-level	MgKα XPS, Fig. 11	
	296 eV	Dy ($4p_{3/2}$, $4p_{5/2}$)-lev.	MgKα XPS	
	1297 eV	Dy $3d_{5/2}$-level	AlKα XPS	
	1335 eV	Dy $3d_{3/2}$-level	AlKα XPS	
E	7.2 eV	S 3p-E_F	ELS, Fig. 12	91K
	13 eV	S 3p-cond. band, surface plasmon	ELS, Fig. 12	
	18.3 eV	bulk plasmon	ELS, Fig. 12	
	27.4 eV	Dy 5p-E_F	ELS, Fig. 12	
	36.1 eV	Dy 5p-5d	ELS, Fig. 12	
	≈ 52 eV	Dy 5s-E_F	ELS, Fig. 12	

phonon wavenumbers

$(\nu/c)_{TO}$	205 cm^{-1}		Raman spectrum	79A
	250 cm^{-1}			
$(\nu/c)_{LO}$	300 cm^{-1}			

dielectric constants

$\varepsilon(0)$	17.1			79A
$\varepsilon(\infty)$	7.8			79A, 79Z

activation energy

E_A	1.5 meV		electrical measurement	77T

electrical conductivity

σ	250 Ω^{-1} cm^{-1}	n-type	see also Fig. 6	67H
	10^{-10} Ω^{-1} cm^{-1}			70H, 82B

Seebeck coefficient

S	50 μV K^{-1}		see also Fig. 7	67H
	120 μV K^{-1}	T = 1300 K		

Further figures and references:

phase diagram: Fig. 1

coordination polyhedra: Fig. 2

thermal conductivity: Fig. 5

Raman spectrum: Fig. 8

absorption spectra: Figs. 3, 9

IR-reflection spectrum: Fig. 4

magnetic properties [67H]

References:

60P Picon, M., Domange, L., Flahaut, J., Guittard, M., Patrie, M.: Bull. Soc. Chim. Fr. 2 (1960) 221.

66H Holtzberg, F., Methfessel, S.: J. Appl. Phys. 37 (1966) 1433.

67H Henderson, J. R., Muramato, M., Loh, E.: J. Chem. Phys. 47 (1967) 3347.

68S Sleight, A. W., Prewitt, C. T.: Inorg. Chem. 7 (1968) 2282.

70H Henderson, J. R. Muramato, M., Gruber, J. B., Menzel, R.: J. Chem. Phys. 52 (1970) 2311.

77T Taher, M. A., Gruber, J. B.: Phys. Rev. B 16 (1977) 1624.

79A Arkatova, T. G., Zhuze, V. P., Karin, M. G., Kamarzin, A. A., Kukharskii, A. A., Mikhailov, B. A., Shelykh, A. I.: Sov. Phys. Solid State 21 (1979) 1979.

79Z Zhuze, V. P., Kamarzin, A. A., Karin, M. G., Sidorin, K. K., Shelykh, A. I.: Sov, Phys. Solid State 21 (1979) 1968.

81K Kamarzin, A. A., Mironov, K. E., Sokolov, V. V., Malovitskii, Y. N., Vasil'yeva, I. G.: J. Cryst. Growth 52 (1981) 619.

82B Batirov, T. M., Verkhovskaya, K. A., Kamarzin, A. A., Malovitskii, Y. N., Lisoivan, V. I., Fridkin, V. M.: Sov. Phys. Solid State 24 (1982) 746.

83S Soldatov, A.V., Gusatinskii, A.N., Karin, M.G., Sidorin, K.K., Sadovskaya, O.A.: Inorg. Mater. 19 (1983) 951-954.

85Z Zhuze, V.P., Karin, M.G., Sidorin, K.K., Sokolov, V.V., Shelykh, A.I.: Sov. Phys. Solid State 27(12) (1985) 2205.

91K Kaciulis, S., Latisenka, A., Plesanovas A.: Surf. Sci. 251/252 (1991) 330.

Fig. 1.

$LnS–Ln_2S_3$ system, Ln = La, Gd, Dy. Phase diagrams [81K].

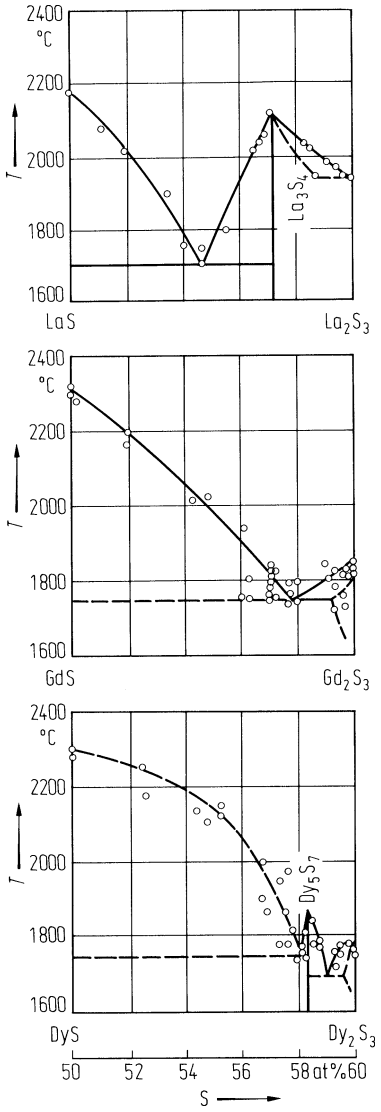

Fig. 2.

Th_3P_4-type compounds. The coordination polyhedra of the cations and the anions. Full circles: Th- atoms, other circles: P-atoms [66H].

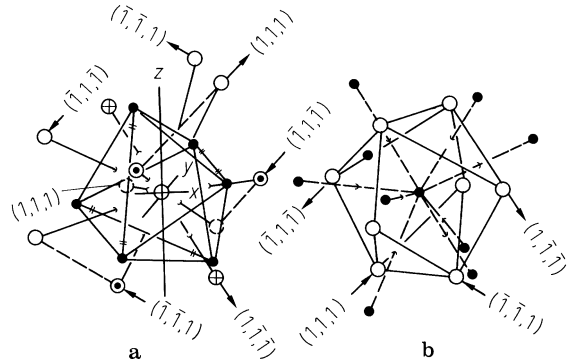

Fig. 3.

γ-La_2S_3, γ-Nd_2S_3, γ-Dy_2S_3. Absorption coefficient vs. photon energy [79Z].

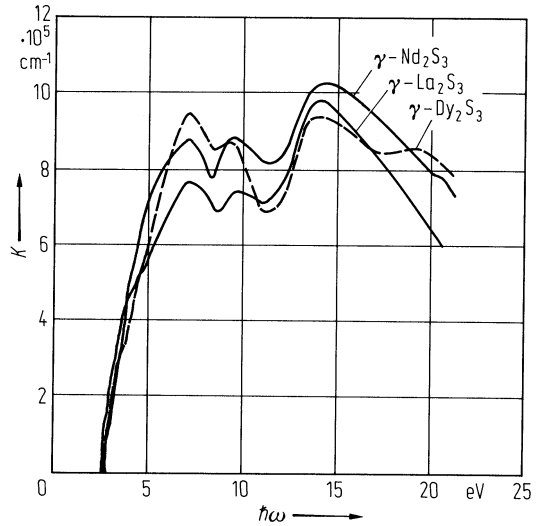

Fig. 4.

γ-La_2S_3, γ-Nd_2S_3, γ-Dy_2S_3. Reflectivity vs. wavenumber in the infrared range [79A].

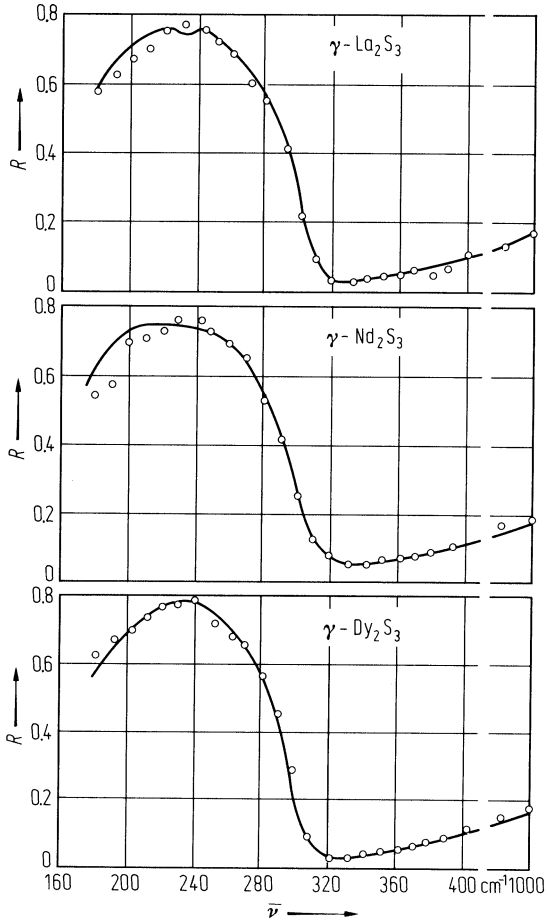

Fig. 5.

γ-Nd_2S_3, γ-Gd_2S_3, γ-Dy_2S_3. Thermal conductivity vs. temperature of several single crystals. The samples show the following excess metal content: Nd_2S_3 (*1*): 0.7% Nd, Nd_2S_3 (*2*): 0.6% Nd, Gd_2S_3 (*1*): 0.4% Gd, Gd_2S_3 (*2*): 0.5% Gd, Dy_2S_3 (*1*): 0.1% Dy, Dy_2S_3 (*2*): 0.2% Dy [77T].

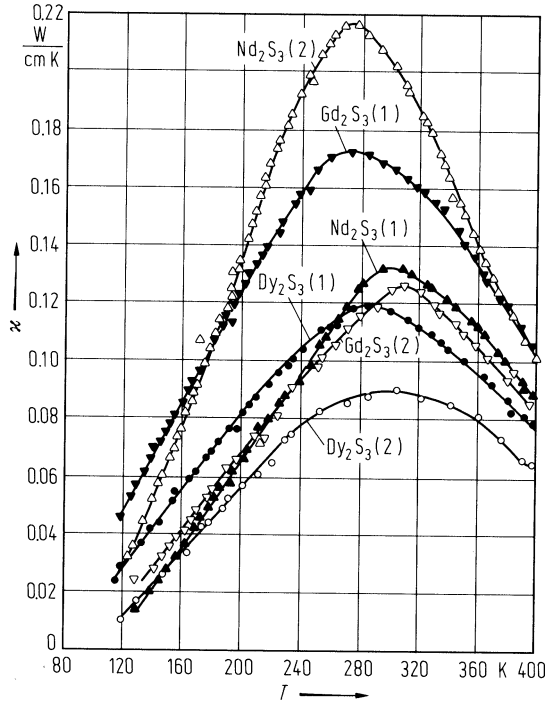

Fig. 6.

γ-Nd_2S_3, γ-Gd_2S_3, γ-Dy_2S_3. Temperature dependence of the electrical conductivity. The sample compositions are given in Fig. 5 [77T].

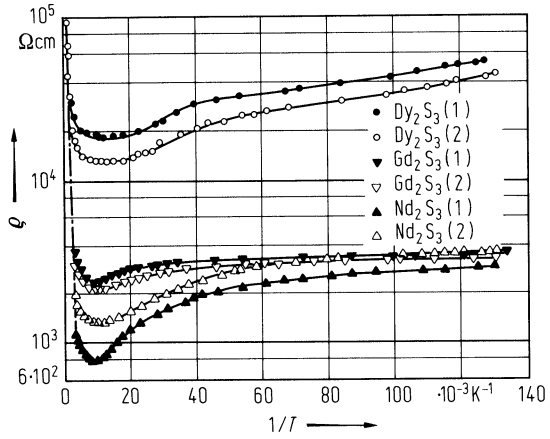

Fig. 7.

γ-Nd_2S_3, γ-Gd_2S_3, γ-Dy_2S_3. Thermoelectric power vs. temperature. The sample compositions are given in Fig. 5 [77T].

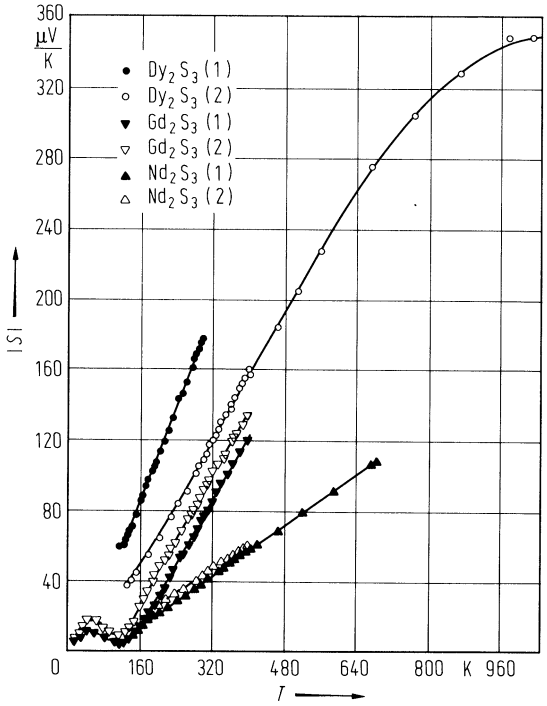

Fig. 8.

γ-Dy_2S_3. Raman intensity vs. Raman shift (in wavenumbers) [79A].

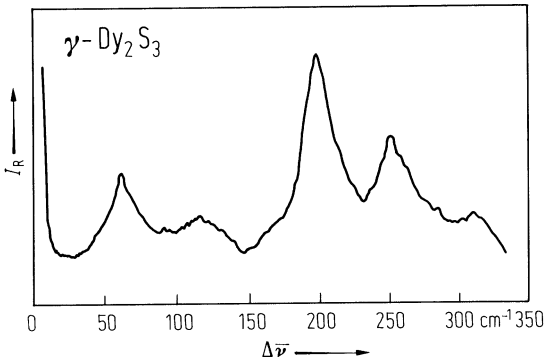

Fig. 9.

γ-Dy_2S_3. Absorption coefficient vs. wavelength for single crystals at 300K [67H].

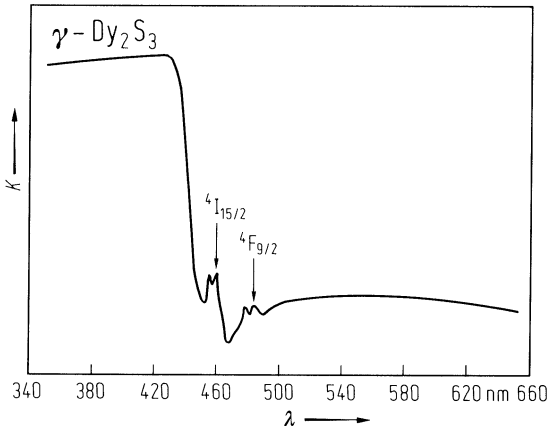

Fig. 10.

γ-Ln_2S_3. MgK_α X-ray photoelectron spectra of the rare-earth sesquisulfides (Ln = La, Ce, Nd, Sm, Gd, Dy) in the energy region below Fermi level down to Ln 5s core level [91K].

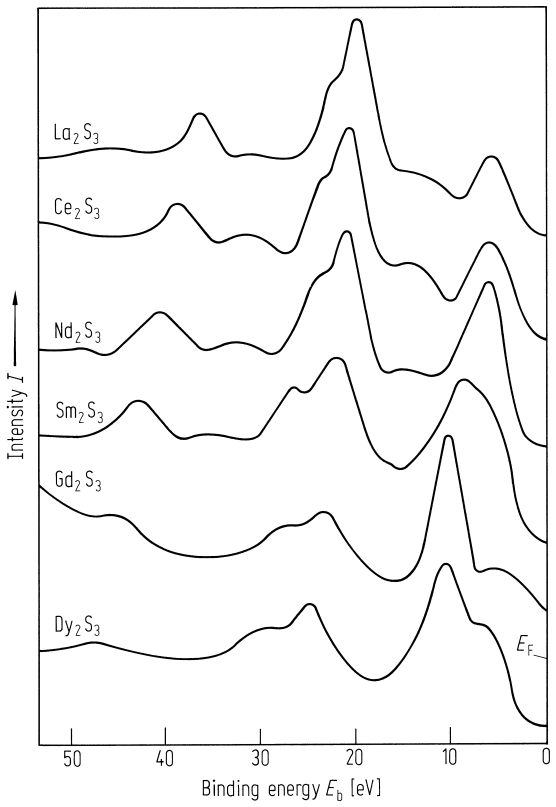

Fig. 11.

γ-Ln_2S_3. MgK_α X-ray photoelectron spectra of the rare-earth sesquisulfides (Ln = La, Ce, Nd, Sm, Gd, Dy) in the 4d core level region [91K]. E_b relative to E_F.

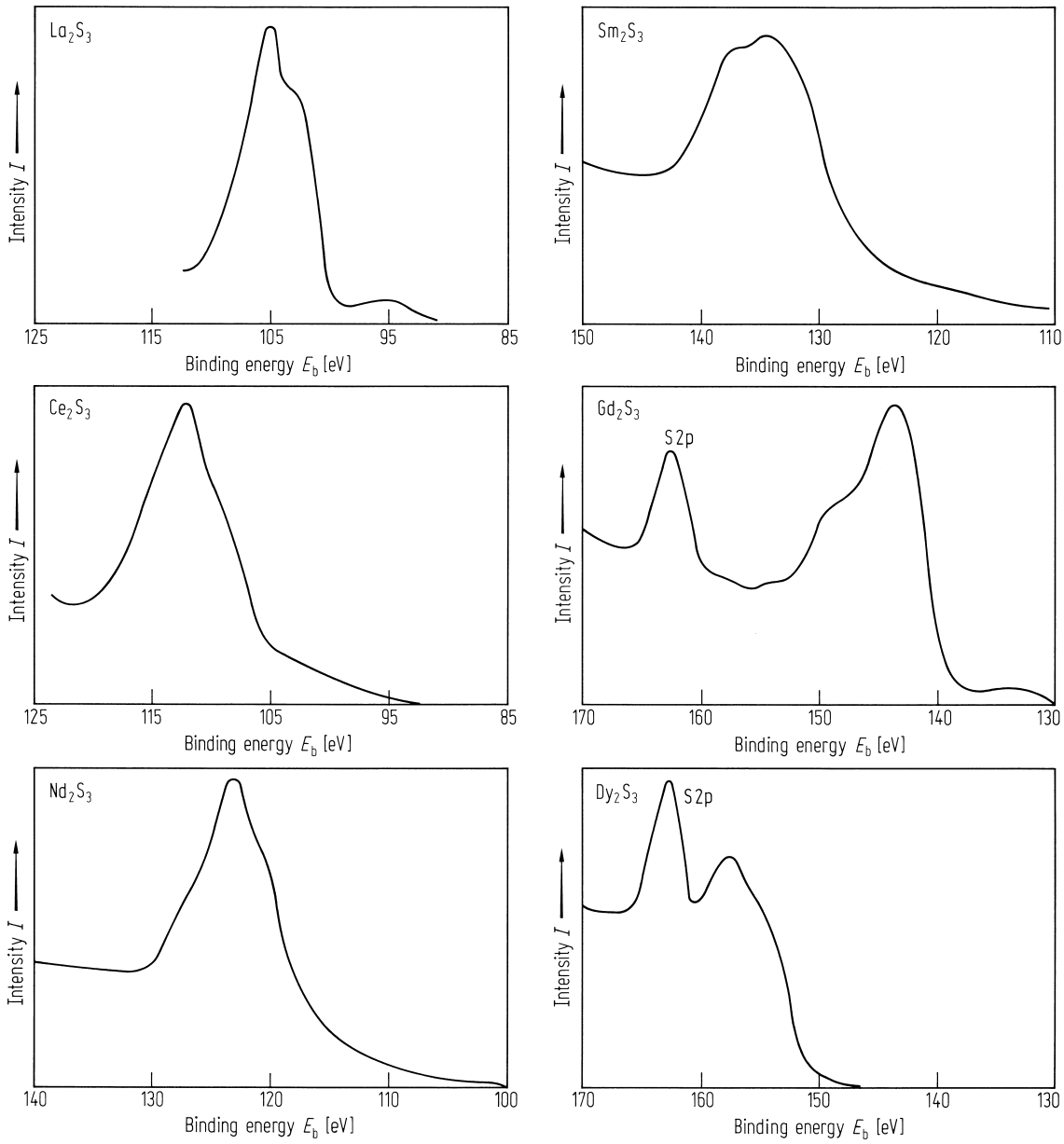

Fig. 12.

γ-Ln_2S_3. Electron loss spectra of the rare-earth sesquisulfides (Ln = La, Ce, Nd, Sm, Gd, Dy) for primary electron beam energy E_p = 750 eV. All the peaks, revealed from the second derivative d^2N/dE^2 are indicated by arrows [91K].